PHYSICAL REVIEW B VOLUME 33, NUMBER 2 15 JANUARY 1986

Raman scattering from coupled plasmon—LO-phonon modes in n-type $Al_xGa_{1-x}As$

T. Yuasa, S. Naritsuka, M. Mannoh, K. Shinozaki, K. Yamanaka, Y. Nomura, M. Mihara, and M. Ishii
Optoelectronics Joint Research Laboratory, 1333 Kamikodanaka, Nakahara-ku, Kawasaki 211, Japan
(Received 29 July 1985)

Raman scattering by coupled plasmon—LO-phonon modes has been studied in direct-band-gap n-type $Al_xGa_{1-x}As$ epitaxial layers with various carrier concentrations. Raman spectra from (100) surfaces of the layers exhibit three branches of the coupled modes whose frequencies and dampings depend on both the carrier concentration and the alloy composition. The dispersion relations of the coupled modes have also been investigated with use of different lines of the excitation lasers, and the wave-vector dependence of the frequencies and dampings have been confirmed. The experimental data agree well with the results calculated by the dielectric-constant method, taking into account the "two-mode" behavior with two sets of the optical phonons in $Al_xGa_{1-x}As$. In addition, the carrier-concentration dependence of the coupled mode strength has been calculated with use of the phonon content as a measure, and compared with the observed one.

I. INTRODUCTION

In a polar semiconductor, the free-carrier plasmons and the longitudinal-optical (LO) phonons are coupled by the interaction between the electric dipole moment due to the relative displacement of the ions and the electric field associated with the free carriers. Such a coupling has been studied theoretically by Varga,[1] Singwi and Tosi,[2] and Burstein *et al.*[3] for the binary compounds consisting of polar optical phonons and degenerate conduction electrons, and experimentally[4–10] by means of the infrared-reflectivity technique and Raman scattering. The infrared-reflectivity measurements are useful as a qualitative guide, and have been applied to analyze the coupled modes in GaAs,[4] CdTe,[4] and GaP.[5] However, they are not quantitative methods, because the frequencies and dampings of the vibrational modes are calculated by fitting the reflectivity data to the theoretical expression with the dielectric function including many adjustable parameters. In Raman scattering experiments one can observe directly the coupled modes. Therefore the frequencies and dampings of the coupled modes are determined accurately. The wave-vector dependence of the coupled modes can be also simply studied in Raman spectra by changing the excitation wavelength.[6,7] The experimental verification of the plasmon-phonon system was performed first by Mooradian and Wright[8] for the Raman spectra of n-type GaAs. They have studied the coupled modes in differently doped samples and have distinguished clear two Raman lines due to the coupling as well as the transverse-optical— (TO-) phonon lines. Their spectra also showed that the frequencies and dampings of the coupled modes change as a function of the free-carrier concentration and the plasma frequency. Thereafter, the Raman spectra from the coupled modes of GaAs and the other binary compounds have been investigated by many researchers.[6,7,9,10] In addition, the coupling between the photoexcited plasmons and the LO phonons have been studied in undoped samples by pulsed Raman scattering.[11]

Although some infrared-reflectivity studies have been reported for the II-VI and III-V alloy systems,[12–14] there have been very few studies of Raman scattering from the plasmon—LO-phonon coupled modes in mixed crystals. Ternary alloy semiconductors are of considerable interest for their applications because they are device materials with a specific band gap and band structure. In III-V ternary semiconductors, $Al_xGa_{1-x}As$ alloys have been the most intensively studied as the most important material for the fabrication of closely-lattice-matched heterojunction optoelectronic devices. The energy-band structure varies with alloy composition from a direct band gap to an indirect band gap. The conduction-electron plasmons couple strongly to the LO phonons in the direct-band-gap region, because the high-density electrons form an electron gas with small effective mass and large dielectric constant.

Recently, we have observed three additional Raman lines of the high-frequency, low-, and intermediate-frequency branches besides the optical phonons in n-type $Al_{0.25}Ga_{0.75}As$ with a high carrier concentration of 1.5×10^{18} cm^{-3}, and identified the lines as the plasmon—LO-phonon coupled modes on the basis of the wave-vector dependence of the modes.[15] The characteristics of the coupled modes in $Al_xGa_{1-x}As$ alloys is the existence of the intermediate-frequency branch, which can never be observed in the binary alloys. The branch originates from "two-mode" behavior, in which two sets of optical phonons with frequencies near those of pure GaAs and pure AlAs are observed over the entire composition range.

In this paper we present the detailed experimental results concerning Raman scattering from the coupled plasmon—LO phonons in n-type $Al_xGa_{1-x}As$ and the theoretical analysis of the frequencies and strengths of the coupled modes as a function of the carrier concentration. This paper is organized as follows. In Sec. II we describe the details of the experimental procedure. The experimental results are presented in Sec. III. In Sec. IV we calculate the coupled-mode frequencies as a function of the carrier concentration using the Drude expression for the

 ©1986 The American Physical Society

dielectric function of the electrons, and the experimental results are discussed in the light of the theoretical calculations. Finally, the dependence of the coupled-mode strengths on the carrier concentration is evaluated by calculating the phonon content of the modes.

II. EXPERIMENTAL

A. Samples

It is necessary, for the study of plasmon-phonon coupling, to use the sample with uniform composition and doping in depth. The *n*-type $Al_xGa_{1-x}As$ layers used in the present study were grown on Cr-doped ⟨100⟩-oriented GaAs substrates by molecular-beam epitaxy (MBE) in a commercial Varian MBE GEN II system, which consists of a growth chamber, a preparation chamber, and a loadlock chamber. The MBE system can provide high-quality $Al_xGa_{1-x}As$ layers having optical and electrical properties comparable to liquid-phase-epitaxial (LPE) layers.[16] In this system it is also possible to precisely control and reproduce beam fluxes, and hence excellent uniformity of the doping profiles as well as the alloy composition is achieved over the whole surface of a substrate. Elemental Al, Ga, As, and Si were used as source material. The group-V (As_4) to group-III (Al + Ga) beam-flux ratio was ~1.5–2.0. The beam fluxes were calculated on the pressure read by the ionization gauge, which can be set directly at the growth position.

The substrates were degreased in organic solvents, rinsed in deionized water, and etched with a 4:1:1 solution of H_2SO_4:H_2O_2:H_2O for 1 min at 30 °C. After a rinse in deionized water, the substrates were dried with nitrogen and mounted with indium on a molybdenum heater block. Then the block was loaded into the MBE system. The substrate temperature during growth was kept at about 730 °C, and it was monitored by a W-Re thermocouple.

Four layers were successively grown on the substrate. An undoped GaAs buffer layer with a thickness of ~1 μm was grown first to obtain a good crystalline quality for succeeding layers. The next layer is a 0.5-μm-thick undoped $Al_xGa_{1-x}As$ buffer layer, followed by a ~3-μm-thick Si-doped *n*-type $Al_xGa_{1-x}As$ layer which is used in the Raman scattering experiment. Finally, a ~300-Å-thick GaAs layer was grown to provide good Ohmic contacts in Hall measurements. The final layer was chemically etched off prior to the Raman scattering measurements. The carrier concentrations of the Si-doped *n*-type $Al_xGa_{1-x}As$ layers were measured by Hall measurements using the van der Pauw technique.

B. Experimental method

The Raman spectra were taken at room temperature in the backscattering geometry. The spectra were observed with chiefly the 514.5-nm line of a Spectra Physics model 164 Ar-ion laser operated at ~200 mW. Some data were taken with the 488.0-nm line of the Ar-ion laser, and with the 530.9- and 568.2-nm lines of a Spectra Physics model 165 Kr-ion laser. These lines were operated at ~100–200 mW. The incident light was focused to a spot about 200 μm in diameter on the surface of the sample. The angle of the incident light was 35°. However, the wave vectors for the incident light inside the crystal are nearly along the direction normal to the surface, because the refractive index for $Al_xGa_{1-x}As$ is so large. The scattered light was collected perpendicularly to the scattering plane by a photographic optics system and focused onto the slit of Jobin-Yvon RAMANOR U-1000 double holographic grating monochromator. The slit widths commonly used gave resolution of ~4 cm^{-1}. The diffracted light was detected by a cooled Hamamatsu R-649 photomultiplier with photon-counting electronics, and the counts were stored in a TRACOR NORTHERN TN-1710 multichannel, analyzer with typical integration times ranging from 0.4 to 0.8 sec and recorded on an *X*-*Y* plotter. The wave-number scale was carefully calibrated by using different lines of a low-pressure Hg lamp, and the Rayleigh and plasma lines in the lasers.

III. EXPERIMENTAL RESULTS

Figure 1 shows the Stokes Raman spectra at room temperature from *n*-type $Al_xGa_{1-x}As$ layers ($x=0$, 0.16, 0.19, and 0.3) with high carrier concentrations. Some additional peaks are observed in addition to LO phonons. For the *n*-type GaAs of Fig. 1(a), a broadband labeled L_+ and a sharp line labeled L_- appear, and these peaks are assigned to the upper and lower longitudinal branches of the coupled plasmon–LO-phonon modes, respectively, because the behavior of the modes coincides with the results, which are well understood for the two coupled modes in heavily doped *n*-type GaAs; at high carrier concentration ($n \gtrsim 1\times10^{18}$ cm^{-3}), the frequency of the upper branch is much higher than the LO-phonon frequency (292 cm^{-1}), while that of the lower branch is closely equal to the TO-phonon frequency (268 cm^{-1}).[8,17] Similar modes are observed in *n*-type $Al_xGa_{1-x}As$ layers. For $Al_xGa_{1-x}As$ ternary alloys, the frequencies of the L_+ modes are higher than those of the AlAs-like LO phonons, and the L_- modes lie near the positions of the GaAs-like TO phonons, which are 267, 266, and 265 cm^{-1} for $x=0.16$, 0.19, and 0.3, respectively. In addition to these two modes, another sharper peak, designated L_0, is observed at intermediate frequency in each $Al_xGa_{1-x}As$ layer. The frequencies of the L_0 modes are nearly equal to those of AlAs-like TO phonons, which are 358, 359, and 360 cm^{-1} for $x=0.16$, 0.19, and 0.3, respectively. Therefore, the L_0 mode can be also interpreted as a branch of the coupled modes. This feature of the L_0 mode has been already reported elsewhere for $x=0.25$.[15] The Raman spectra also show the optical-phonon groups due to second-order processes, which are labeled *H* in Fig. 1.

In order to perform a detailed study of the plasmon–LO-phonon coupling in *n*-type $Al_xGa_{1-x}As$, we investigated the Raman scattering from the differently doped *n*-type $Al_xGa_{1-x}As$ layers with fixed Al molar fraction. The Raman spectra from *n*-type $Al_{0.19}Ga_{0.81}As$ layers are shown in Fig. 2 for carrier concentrations of 1.7×10^{17}, 7.1×10^{17}, 8.8×10^{17}, and 3.7×10^{18} cm^{-3}. The carrier concentrations in the figure are the results from the Hall measurements. Only two LO phonons, one "GaAs-like"

and the other "AlAs-like," are observed in the sample with the lower carrier concentration of $n=1.7\times10^{17}$ cm^{-3}. The two LO-phonon modes are sharp, but their half-widths are somewhat wider than those of the LO phonons in the pure compounds GaAs and AlAs. In addition, each mode has a lower-energy tail which forms the asymmetric profile. This asymmetry is most probably due to disorder-activated modes of the LO branch with a wave vector in the proximity of $k=0$, as discussed in Ref. 12. When n increases to 7.1×10^{17} cm^{-3}, two shoulders, labeled L_+ and L_0, appear on the high-frequency side of

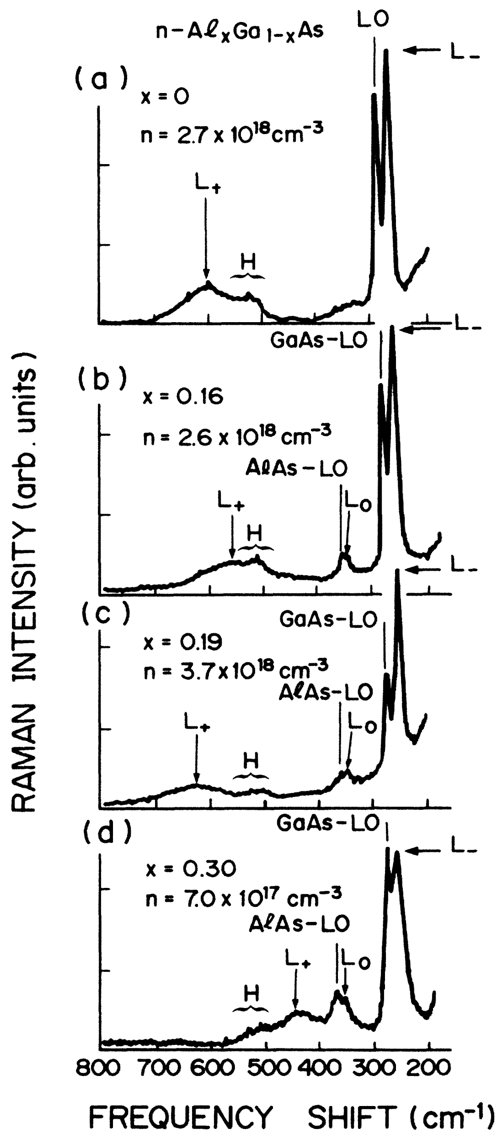

FIG. 1. Raman spectra from (100) surfaces of heavily doped direct-band-gap n-type $Al_xGa_{1-x}As$ layers with different alloy compositions. These spectra were obtained with the 514.5-nm line of an Ar-ion laser. The arrows labeled L_+, L_0, and L_- represent the coupled plasmon—LO-phonon modes. Sharp structures, labeled LO, GaAs-LO, and AlAs-LO are the LO phonon of pure GaAs, and the GaAs and AlAs-like modes of the LO phonons in $Al_xGa_{1-x}As$. Some broad peaks labeled H are the second-order phonon modes.

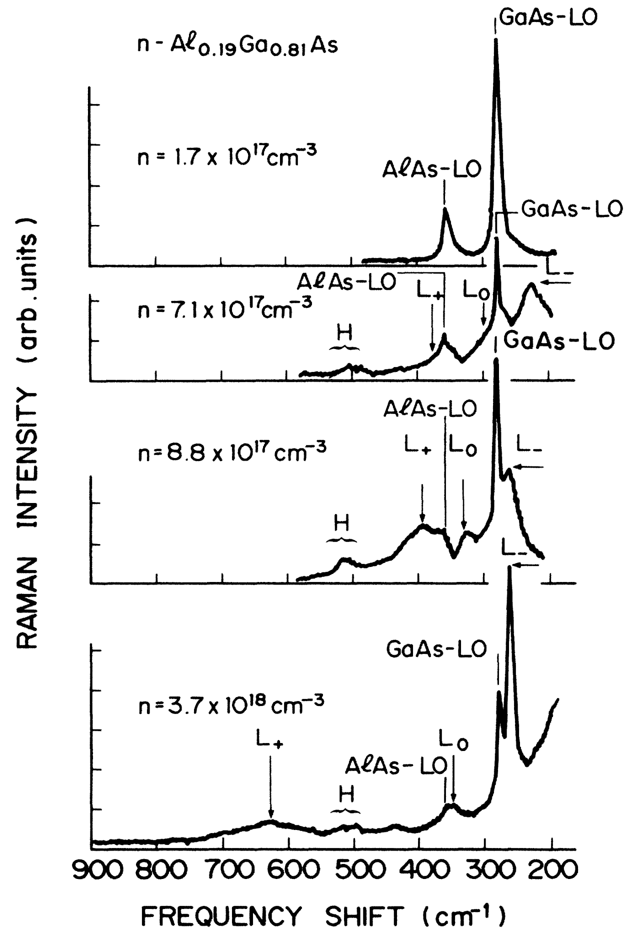

FIG. 2. Raman spectra from (100) n-type $Al_{0.19}Ga_{0.81}As$ layers with carrier concentrations ranging from 1.7×10^{17} to 3.7×10^{18} cm^{-3}. The measurements were made using the 514.-5-nm laser line. Both of the two LO phonons from the depletion layer and the coupled modes L_+, L_0, and L_- are observed. The sample with $n=3.7\times10^{18}$ cm^{-3} is the same as that of Fig. 1(c).

each LO phonon, and a broader mode, denoted L_-, is also observed on the low-frequency side of the GaAs-like LO phonon. The alloy composition is determined by the frequencies of the two LO phonons originating from the surface-depletion layers. For the sample with $n=8.8\times10^{17}$ cm^{-3}, the L_+ and L_0 modes are clearly separated from each LO-phonon peak, and the L_- mode sharpens. At the highest carrier concentration, $n=3.7\times10^{18}$ cm^{-3}, the L_- and L_0 modes vibrate at the GaAs-like and the AlAs-like TO-phonon frequency, respectively, while the L_+ mode shifts to still higher frequency.

The same studies were performed for other alloy compositions. The behavior of the coupled mode for $x=0.3$ in Fig. 3 is similar in the carrier concentration dependence of their frequencies to that for $x=0.19$ in Fig. 2. Comparing Fig. 3 with Fig. 2, the coupled modes in the layers with $x=0.3$ seem to be clearly separated from the LO phonons at lower carrier concentrations. This fact, however, is not reasonable, because the plasma frequency de-

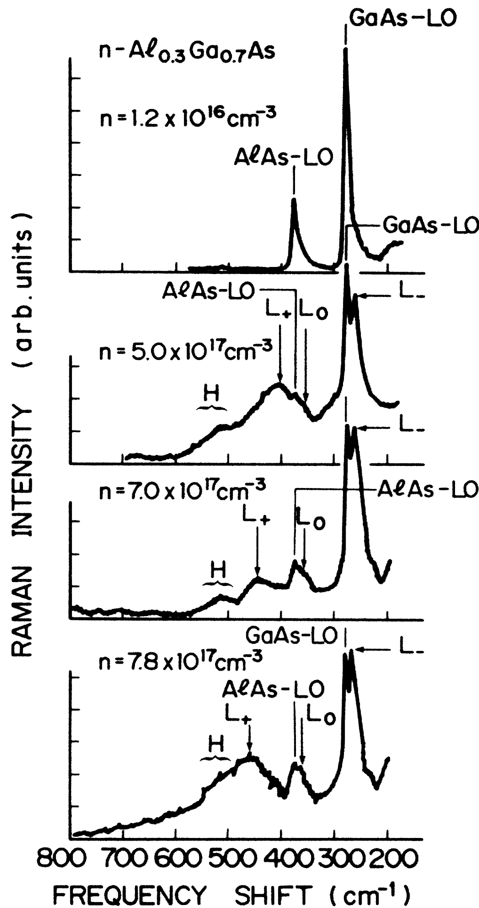

FIG. 3. Raman spectra from (100) n-type $Al_{0.3}Ga_{0.7}As$ layers with carrier concentrations ranging from 1.2×10^{16} to 7.8×10^{17} cm^{-3}. The 514.5-nm line was used. The sample with $n=7.0\times10^{17}$ cm^{-3} is the same as that of Fig. 1(d).

creases with increasing Al content with the larger effective mass[18] of the conduction electrons. This discrepancy can be possibly explained by the excess conduction electrons in the n-type $Al_{0.3}Ga_{0.7}As$ layer, which are optically pumped from the deep traps by the laser excitation. It is well known that an increase of the Al content to $0.3<x<0.4$ in Si-doped n-type $Al_xGa_{1-x}As$ leads to a drastic reduction of Hall electron concentration. Various mechanism have been reported in the literature to account for this behavior.[19–21] The most possible explanation is that with increasing x the Hall electron concentration no longer corresponds to overall Si-impurity concentration, because a certain amount of Si atoms is participating in the formation of deep donor-type traps, as first proposed by Lang *et al.*[20] At high carrier concentrations, electrons are captured in the traps even at room temperature.[22] If we accept this explanation, in Raman scattering experiments the captured electrons in the deep traps could be released under the high electric field of the laser excitation and result in the increase in the number of conduction electrons.

The coupled plasmon–LO-phonon modes depend on the scattering wave vector because of dispersion effects in plasmons. Such a wave-vector dependence of the coupled modes has been studied particularly for n-type.[6,7] The wave vectors of the elementary excitations can be varied by changing the energy of the incident photons through the relationship between the wave vector, the photon frequency, and the frequency-dependent refractive index. In order to investigate the wave-vector dependence of the coupled modes in n-type $Al_xGa_{1-x}As$, we have measured Raman scattering using various emission lines of Kr-ion and Ar-ion lasers in the (~488.0–503.5)-nm range.

Figure 4 shows the Raman spectra in n-type $Al_{0.25}Ga_{0.75}As$ with $n=1.5\times10^{18}$ cm^{-3} at four different laser-excitation wavelengths λ, i.e., scattering wave vectors. Both the frequencies and dampings of the coupled modes vary with the excitation wavelength, as seen in Fig. 4. Each coupled mode shifts to higher frequencies with increasing wave vector. The frequency shift of the L_+ mode is more remarkable than those of the L_0 and L_- modes, that is, the shift is about 10 cm^{-1} for the L_+

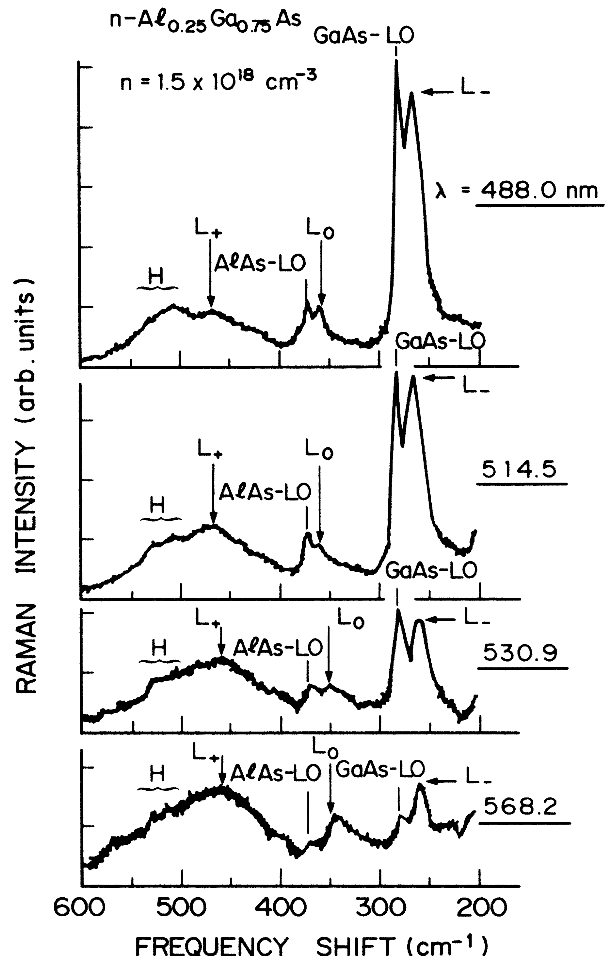

FIG. 4. Raman spectra from n-type $Al_{0.25}Ga_{0.75}As$ with $n=1.5\times10^{18}$ cm^{-3} at four different laser-excitation wavelengths (λ). The frequencies of the coupled modes increase with decreasing excitation wavelength. The intensity ratio of the L_+ mode to the L_- (or L_0) mode also depends on the excitation wavelength.

mode and about ~2–3 cm^{-1} for the L_0 and L_- modes. These dispersion relations are like those of the coupled modes in n-type GaAs. The higher-frequency coupled mode shifts to higher frequencies with increasing wave vector for a given free carrier concentration in n-type GaAs, and the low-frequency mode also shifts to higher frequencies, approaching the LO-phonon frequency within the free-particle excitation spectrum. In particularly, at the limit of high carrier concentration, as indicated by Varga's theoretical results, the high-frequency coupled mode in n-type GaAs is pure plasmon, which depends strongly on the wave vector, and the low-frequency mode is pure optical phonon, the dispersion of which can be neglected because of the very small wave vector compared to the Brillouin-zone boundary vector. Varga's results explain the difference in the frequency shifts between the coupled modes in Fig. 4, since the L_0 mode is plasmonlike, while the L_0 and L_- modes are phononlike.

In order to clarify the wave-vector dependence of the intensity of each coupled mode, the spectra in Fig. 4 were replotted, excluding two LO phonons as shown in Fig. 5. In Fig. 5 the peak heights of the L_+ and L_0 modes are normalized to that of the L_- mode. The intensity ratio of L_+/L_- decreases intensively with increasing wave vector. This change can be understood by the dependence of Raman scattering cross section on the ratio of phonon content to plasmon content in the plasmon-phonon system. The cross section increases upon increasing the phonon content over the plasmon content.[9,23] As the wave vector increases, the L_+ mode becomes more plasmonlike and the L_- mode becomes more phononlike, as described above. Accordingly, the scattering intensity of the L_+ mode decreases and that of the L_- mode increases.

Figure 5 also shows the slight increase in the intensity ratio of L_0/L_- with increasing wave vector, indicating the different wave-vector dependence between the L_0 and L_- modes. However, the difference is slight. This is due

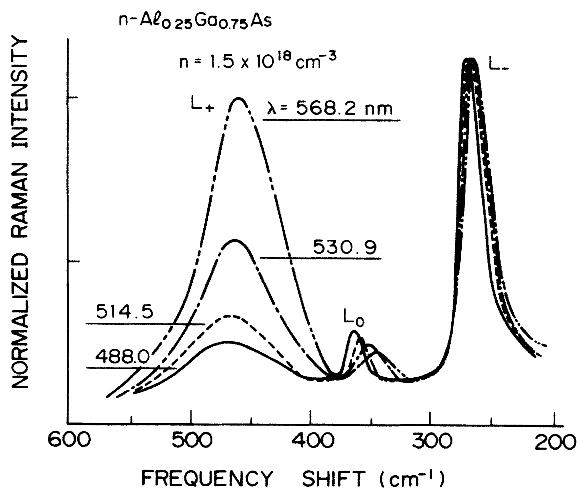

FIG. 5. The coupled modes in Fig. 4 are rewritten, and each peak intensity of the L_- mode is normalized to unity. The intensity ratio of the L_+ to L_- (or L_0) mode becomes smaller with decreasing excitation wavelength.

to the fact that the behavior of the L_0 mode in this case is essentially same as that of the L_- mode, since both modes at high carrier concentration are phononlike. These dispersion effects experimentally confirm the existence of three coupled modes in n-type $Al_xGa_{1-x}As$. Furthermore, the coupling between the plasmons and LO phonons in ternary alloys with "two-mode behavior" are discussed theoretically in the following.

IV. THEORY AND DISCUSSIONS

A. Coupled-mode frequencies

1. Theoretical calculation

We consider the combined plasmon-phonon system by the dielectric constant method, first employed for binary polar semiconductors by Verga.[1] The method assumes that the polarizabilities of the ion system and the electron system are additive, that is, the polarization of the coupled system is the sum of the electronic and ionic parts. The lattice polarization P_L and electron polarization P_e are given by the following equations:

$$P_L=(4\pi)^{-1}[\epsilon_L(\omega)-1]E \ , \tag{1}$$

$$P_e=(4\pi)^{-1}[\epsilon_e(q,\omega)-1]E \ , \tag{2}$$

where $\epsilon_L(\omega)$ is the frequency- (ω) dependent dielectric function of the lattice, $\epsilon_e(q,\omega)$ is the wave-vector- (q-) and frequency-dependent dielectric function of an electron gas, and E is the electric field. The total polarization of the system is given by

$$P_T=(4\pi)^{-1}[\epsilon_T(q,\omega)-1]E \ . \tag{3}$$

On the above assumption,

$$P_T=P_L+P_e=(4\pi)^{-1}[\epsilon_L(\omega)+\epsilon_e(q,\omega)-2]E \ . \tag{4}$$

From Eqs. (1)–(4) the total dielectric function of the system is

$$\epsilon_T(q,\omega)=\epsilon_L(\omega)+\epsilon_e(q,\omega)-1 \ . \tag{5}$$

When the electrons form a degenerate Fermi gas, and the screening length is small, the Lindhard dielectric function[2] is an accurate approximation for the dielectric function of the electron gas in the system. The expression, when expanded in powers of the wave vector, is

$$\epsilon_e(q,\omega)=1-\frac{\omega_p^2}{\omega^2}\epsilon_\infty\left[1+\frac{3}{5}\frac{v_0^2}{\omega^2}q^2+\cdots\right] , \tag{6}$$

where ω_p is the plasma frequency when the electron interactions are screened, ϵ_∞ is the high-frequency dielectric constant, v_0 is the Fermi velocity, $v_0=\hbar k_F/m^*$, $k_F=(3\pi^2 n)^{1/3}$, m^* is the effective mass of the electrons, and n is the carrier concentration. We treat the case in which all electrons are in the parabolic central valley, and then

$$\omega_p^2=4\pi ne^2/m^*\epsilon_\infty \ . \tag{7}$$

For $\omega\sim\omega_p \gg qv_0$, Eq. (6) can be approximately written as

$$\epsilon_e(q,\omega)=1-\frac{\epsilon_\infty}{\omega^2}\omega_p^2(q) , \quad (8)$$

$$\omega_p^2(q)=\omega_p^2+\tfrac{3}{5}(v_0 q)^2 . \quad (9)$$

The frequencies of the coupled modes are given by the roots of the total dielectric function. This dielectric constant method has been already employed in the analysis of the coupled modes in GaAs and other binary alloys.[8,9,11,17]

The behavior of the coupled modes in $Al_xGa_{1-x}As$ is different from that in binary alloys since $Al_xGa_{1-x}As$ exhibits two separate optical-phonon branches, as presented in Sec. III. The dielectric function of the lattice in $Al_xGa_{1-x}As$ is

$$\epsilon_L(\omega)=\epsilon_\infty+\sum_{j=1}^{2} S_j/[1-(\omega/\omega_{tj})^2] , \quad (10)$$

where $j=1$ and 2 refer to GaAs-like and AlAs-like branches, respectively. Phonon dampings are neglected in Eq. (10). ω_{tj} is the TO-phonon frequency and S_j is the jth oscillator strength. The coupled-mode frequencies ω_Z are derived by equating the total dielectric function to zero. The equations $\epsilon_T(q,\omega)=0$, (5), (8), and (10) lead to the following equation,

$$\frac{\epsilon_\infty}{(\omega_{t1}\omega_{t2})^2}\omega^6-\left[\epsilon_\infty\left[\frac{1}{\omega_{t1}^2}+\frac{1}{\omega_{t2}^2}\right]+\left[\frac{S_1}{\omega_{t2}^2}+\frac{S_2}{\omega_{t1}^2}\right]+\frac{\epsilon_\infty\omega_p^2(q)}{(\omega_{t1}\omega_{t2})^2}\right]\omega^4 + \left[\epsilon_\infty+S_1+S_2+\epsilon_\infty\omega_p^2(q)\left[\frac{S_1}{\omega_{t1}^2}+\frac{S_2}{\omega_{t2}^2}\right]\right]\omega^2-\epsilon_\infty\omega_p^2(q)=0 . \quad (11)$$

The solutions of Eq. (11) give ω_Z. The oscillator strengths S_1 and S_2 are obtained as the solutions of the following equations:

$$S_1+S_2=\epsilon_\infty[(\omega_{l1}\omega_{l2}/\omega_{t1}\omega_{t2})^2-1] , \quad (12)$$

$$(1+S_1/\epsilon_\infty)\omega_{t1}^2+(1+S_2/\epsilon_\infty)\omega_{t2}^2=\omega_{l1}^2+\omega_{l2}^2 , \quad (13)$$

where ω_{l1} and ω_{l2} are the GaAs-like and AlAs-like LO-phonon frequencies, respectively. For $Al_xGa_{1-x}As$, the effective mass of the electrons in the Γ valley, m^*, changes with the alloy composition x as follows:[18]

$$m^*/m_0=0.0636+0.0552x+0.0092x^2 . \quad (14)$$

The alloy-composition dependence of ϵ_∞ is given by a linear assumption,

$$\epsilon_\infty=(1-x)\epsilon_\infty(\mathrm{GaAs})+x\epsilon_\infty(\mathrm{AlAs}) = 11.1-2.83x . \quad (15)$$

The conduction band of $Al_xGa_{1-x}As$ is nonparabolic and, therefore, the effective mass depends on the carrier concentration. However, no reliable data have been published for the carrier-concentration dependence of the effective mass all over the alloy composition. On the other hand, the data for GaAs have been presented in the literature.[24] For simplicity, we assumed that the effective mass in the conduction band of $Al_xGa_{1-x}As$ has the same carrier-concentration dependence as for GaAs. The optical-phonon frequencies ω_{lj} and ω_{tj} also depend on the alloy composition. Thus, if the alloy composition and the wave vector, i.e., the excitation wavelength, are given, the coupled-mode frequencies can be calculated as a function of both the carrier concentration and the alloy composition.

Figure 6 is an example of the calculated curves of the carrier-concentration dependence of the coupled-mode frequencies in n-type $Al_xGa_{1-x}As$. The calculation is carried out for $x=0.2$. The curves are shown as a function of the square root of the carrier concentration for the 514.5-nm line of an Ar-ion laser. The wave-vector-dependent plasma frequency $\omega_p(q)$ is also shown as a solid line, which is nearly linear over the wide region of the carrier concentration. As shown in Fig. 6, there exist three new normal modes (labeled L_+, L_0, and L_-) in the plasmon-phonon system. On the other hand, only two coupled modes are allowed in degenerate GaAs. In Fig. 6, when the carrier concentration increases, the high-frequency mode L_+ (frequency ω_+) shifts from the AlAs-like LO-phonon position to the higher-frequency side, the low-frequency mode L_- (frequency ω_-) approaches the GaAs-like TO-phonon position, and the intermediate-frequency mode L_0 (frequency ω_0) shifts

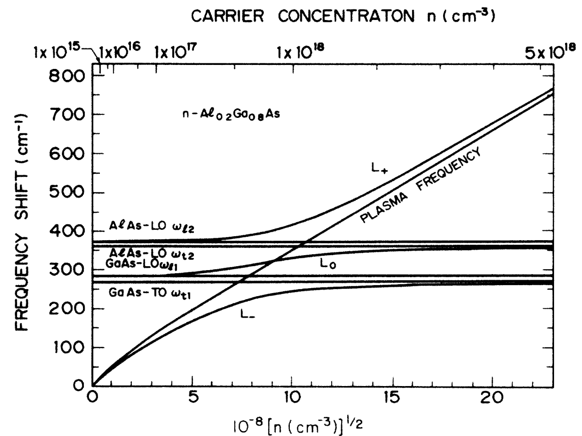

FIG. 6. Calculated shifts of the coupled-mode frequencies in n-type $Al_{0.2}Ga_{0.8}As$ for 514.5-nm excitation as a function of the square root of the carrier concentration. The plasma frequency is also given. The GaAs-like TO-, LO-, AlAs-like, TO; and LO-phonon frequencies denoted ω_{tl}, ω_{l1}, ω_{t2}, and ω_{l2} are 266.5, 283.0, 360.2, and 372.5 cm^{-1}, respectively.

from the GaAs-like LO-phonon position to the AlAs-like TO-phonon position. At low carrier concentration ($n \lesssim 1\times10^{16}$ cm^{-3}), the L_- mode is a plasmonlike mode in which the displacements of the carriers are partly screened by ion displacements, and the L_+ and L_0 modes are phononlike modes with $\omega_+ \sim \omega_{AlAs\text{-}LO}$ and $\omega_0 \sim \omega_{GaAs\text{-}LO}$, respectively. In contrast, at high carrier concentration ($n \gtrsim 2\times10^{18}$ cm^{-3}), the L_+ mode is plasmonlike in character with $\omega_+ \sim \omega_p(q)$, and the L_0 and L_- modes are phononlike with $\omega_0 \sim \omega_{AlAs\text{-}TO}$ and $\omega_- \sim \omega_{GaAs\text{-}TO}$, in which the displacements of the ions are completely screened by the electron displacements.

The wave-vector dependence of the dielectric function of the electron gas as expressed in Eq. (8) leads to the dispersion of the coupled-mode frequencies. In Fig. 7 the calculated behavior of the coupled-mode frequencies in n-type $Al_{0.2}Ga_{0.8}As$ versus the carrier concentration is shown for the strong lines of Ar-ion and Nd-ion YAG (yttrium-aluminum-garnet) lasers. For a given carrier concentration, the coupled modes shift to higher frequencies with increasing excitation wavelength, i.e., the wave vector. The frequency dispersions of the L_+, L_0, and L_- modes are clearly observed in the low-, intermediate-, and high-carrier-concentration ranges, respectively, as seen in Fig. 7. When the wave vector becomes large enough to penetrate into the Landau damping region, where the plasmon decays into a single particle-hole pair, the L_+ mode becomes overdamped, and the L_0 and L_- modes would approach the AlAs-like and GaAs-like LO phonons, respectively, as indicated in n-type GaAs. The coupled-mode frequencies in the Landau damping region can be calculated using the dielectric function including the imaginary part, because the damping is expressed by the imaginary part of the longitudinal dielectric function of the electron gas. The cutoff wave vector q_c above which the coupled mode comes into the Landau damping region is given by $\omega = q_c v_F + \hbar q_c^2/2m^*$ for a given ω. For the wave vectors used in Fig. 7, the L_+ mode is outside the Landau damping region and the L_0 model is also almost outside the region; on the other hand, the L_- mode excited with the visible laser lines extends slightly into the Landau damping region at $n > 1\times10^{17}$ cm^{-3}. However, the dispersion relation of the L_- mode is almost unchanged because the frequency shift due to the Landau damping is small near the boundary of the single-particle excitation region.[1]

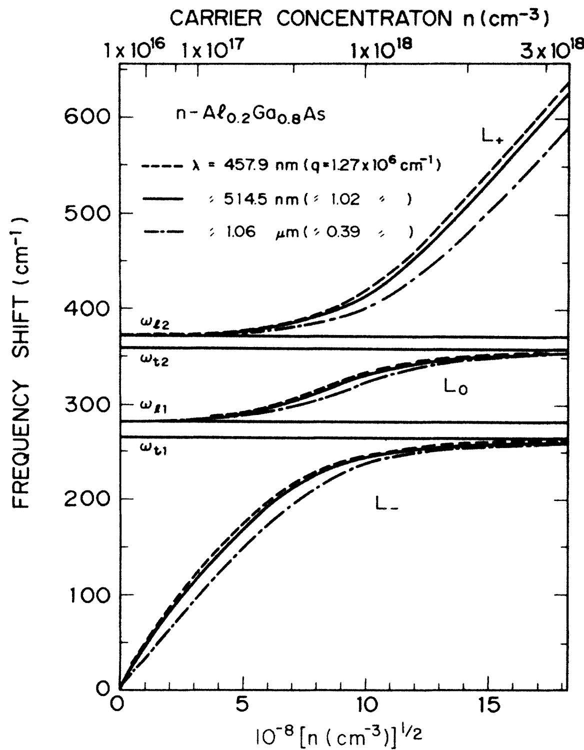

FIG. 7. The dependence of the calculated frequencies of the coupled modes in n-type $Al_{0.2}Ga_{0.8}As$ on the carrier concentration is shown for three excitation wavelengths. The curve for 514.5 nm is the same as that in Fig. 6.

The L_--mode frequency depends strongly on the carrier concentration in the region $1\times10^{16} \lesssim n \lesssim 5\times10^{17}$ cm^{-3}, as shown in Figs. 6 and 7. In the visibly excited Raman scattering spectra, the L_- mode in this carrier-concentration range cannot be clearly observed because the penetration depth is comparable to or larger than the depth of the surface-depletion layer. This limitation is eliminated by using infrared light, which passes through the AlGaAs layer transparently. The infrared excitation would also improve the observability of the L_+ and L_0 modes by decreasing, relatively, the LO-phonon signals, because the signals obscure the clear appearance of the coupled modes.

2. *Comparison of theory with experiment*

The experimental results for the coupled-mode frequencies are compared with the numerically calculated values. The solid curves in Fig. 8 show the calculated frequencies of n-type $Al_{0.19}Ga_{0.81}As$ as a function of carrier concen-

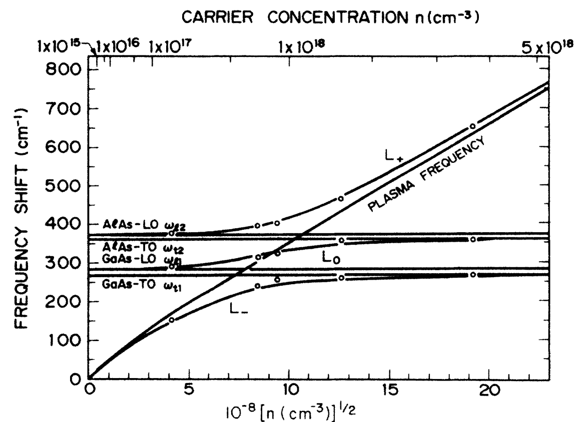

FIG. 8. The experimental results of the carrier-concentration dependence of the coupled-mode frequencies in n-type $Al_{0.19}Ga_{0.81}As$ are compared with the calculated values. The solid curves show the calculated coupled-mode frequencies as a function of the square root of the carrier concentration. The observed coupled-mode frequencies are plotted as open circles. The excitation wavelength is 514.5 nm.

tration. Also plotted are measured peak frequencies from samples with various carrier concentrations. The experimental results agree well with the calculated ones, although in the calculation the one-conduction-band model of the Γ valley is used and the plasma damping is neglected. The validity of these assumptions is discussed as follows. Generally, for electron conduction in *n*-type $Al_xGa_{1-x}As$, three valleys, Γ, *L*, and *X*, should be taken into account. However, most of electrons for $x=0.19$ are present in the Γ valley, and the electron plasma in the valley dominates the plasmon-phonon coupling because the Γ conduction-band minimum is much lower in energy than the conduction-band minima at the *X* and *L* points, and the effective mass of electrons in the Γ valley is an order of magnitude smaller than those in other valleys. Therefore, the one-conduction-band model is applicable for the calculation of the coupling frequencies of *n*-type $Al_{0.19}Ga_{0.81}As$. Chang *et al.*[25] calculated the fraction of electrons in the Γ, *L*, and *X* valleys, and the ratio of the true electron concentration (n_T), as a function of the alloy composition. According to their results, the ratio of the carrier concentration in the Γ valley (n_Γ) to n_T is 0.96 for $x=0.19$, and that of n_T to n_H is 1.0, that is, $n_\Gamma=0.96n_H$. Thus, the electrons concentrate in the Γ valley.

The plasma damping is inversely proportional to the carrier mobility. The mobility of *n*-type GaAs is so high that the damping can be neglected for the calculation of the coupled-mode frequencies. Such a high mobility value is kept in the direct-band-gap region of *n*-type $Al_xGa_{1-x}As$ with an alloy composition of $x \lesssim 0.3$. Accordingly, the assumption of negligible plasma damping is allowable for the calculation in *n*-type $Al_{0.19}Ga_{0.81}As$.

As the alloy composition approaches the direct-indirect band-gap crossover point, the conduction electrons in the *L* and *X* valleys increase upon increasing the contributions of the plasmas in those valleys to the plasmon-phonon coupling. Furthermore, at high Si-doping densities, it is possible that the photoexcited electrons from the deep donor traps participate in the coupling, increasing the carrier concentration in the Γ valley. In addition, the mobility decreases steeply for the alloy composition of $x>0.3$, producing the large plasma-damping constant which shifts the coupled-mode frequencies through the imaginary part of the dielectric constant. Thus, the plasma damping cannot be neglected, and the one-conduction-band model of the valley should be modified. The evaluation of the carrier increases by photoexcitation requires the correct solution of the electron distribution among the valleys under laser excitation, which is not clear at present time.

B. Coupled-mode strengths

We investigate the squared matrix element for the phonon as a qualitative measurement of the coupled-mode intensity. The scattering cross section of the coupled mode, i.e., the coupling strength, is approximately proportional to the phonon content, defined as $S_m = |\langle m | \varphi_q | 0\rangle|^2$, where $|0\rangle$ is the ground state, $\langle m|$ is a one-quantum excited state of mode *m*, and $\varphi_q = b_q + b^\dagger_{-q}$, where b_q and $b^\dagger_q$ are, respectively, the phonon destruction and creation operators. Varga[1] has introduced S_m as phonon strength to denote the distribution of energy which is phononlike, and derived the expression for S_m in the diatomic ionic crystals as a function of coupled-mode frequency. We apply his procedure to the phonon content of the coupled modes in the ternary crystals, and obtain the following expression for the phonon content $S_m(q)$:

$$S_m^{-1}(q) = \frac{\omega_m}{\omega_{lj}} + \frac{S_j\omega_j^2}{\omega_{lj}} \frac{\omega_p^2(q)\omega_m}{\epsilon_\infty[\omega_m^2-\omega_p^2(q)]^2} . \quad (16)$$

The details of Eq. (16) are discussed in Appendix. In Eq. (16), the ω_m are the coupled-mode frequencies, and the phonon contents of the L_- and L_+ modes are represented by $j=1$ and 2, respectively. The phonon content of the L_0 mode is calculated by using ω_{l1} at low carrier concentration, ω_{l2} at high carrier concentration, and both frequencies at intermediate carrier concentration. In the limit of the pure phonon, we have $S=1$. On the other hand, in the limit of the pure plasmon, we have $S=0$.

The phonon contents of the coupled modes in *n*-type $Al_{0.2}Ga_{0.8}As$ are plotted as a function of carrier concentration in Fig. 9. They were calculated from Eq. (16) with an excitation wavelength of 514.5 nm. For simplicity, only the GaAs-like LO-phonon frequency was used in the calculation of the phonon content of the L_0 mode. The curves for the L_+ and L_- modes are similar to those for two branches of the coupled modes in *n*-type GaAs. In the low-carrier-concentration range, $S_- \ll 1$ and $S_+ \sim 1$, i.e., the L_- mode is plasmonlike, and the L_+ mode is almost the AlAs-like LO phonon. In the high-carrier-

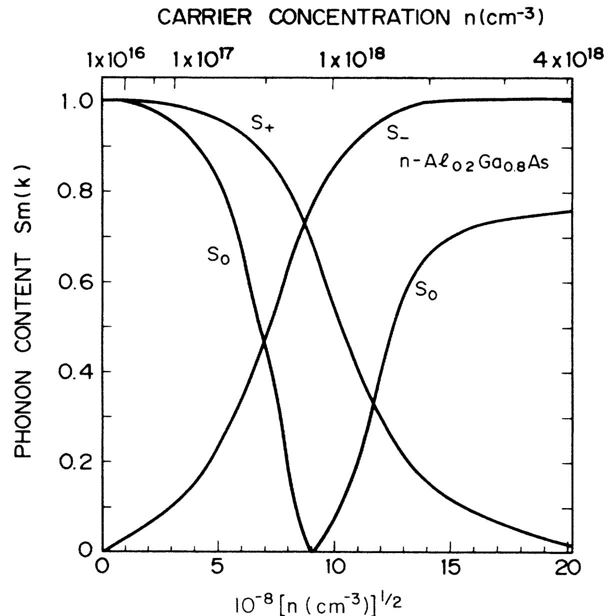

FIG. 9. Calculated phonon content of the coupled modes in *n*-type $Al_{0.2}Ga_{0.8}As$ for 514.5-nm excitation as a function of the square root of the carrier concentration. The phonon content of the L_+, L_0, and L_- modes is designated S_+, S_0, and S_-, respectively. The L_0-mode frequency is equal to the plasma frequency at the L_0 minimum.

concentration range, $S_- \sim 1$ and $S_+ \ll 1$, i.e., the L_- mode is almost the GaAs-like LO phonon, and the L_+ mode is plasmonlike. The behavior of S_0 is not monotonous, but has a minimum. At low carrier concentration, the L_0 mode contains the large GaAs-like LO-phonon content with $S_0 \sim 1$. At high carrier concentration it should contain the large AlAs-like LO-phonon content with $S_0 \sim 1$. However, even at the highest carrier concentration the phonon content is less than unity, as shown in Fig. 9. This discrepancy can be solved by using the AlAs-like LO-phonon frequency instead of the GaAs-like LO-phonon frequency instead of the GaAs-like LO-phonon frequency at high carrier concentration. At intermediate carrier concentration the plasmons contribute strongly to the plasmon-phonon mixing in the L_0 mode, decreasing the phonon content. Figure 9 shows the S_0 minimum of zero value at the intermediate carrier concentration. At the minimum point the L_0-mode frequency is equal to the plasma frequency, as indicated by Eq. (16).

The coupled-mode half-width, which corresponds to mode damping, is approximately in inverse proportion to the phonon content of the mode. Therefore, the calculated phonon-content curves in Fig. 9 can be examined by using the coupled-mode half-widths. Figure 10 shows a plot of the reciprocals of the normalized coupled-mode half-widths for n-type $Al_{0.19}Ga_{0.81}As$ as a function of the carrier concentration. For the normalization, the GaAs and AlAs-like LO phonons are used for the L_0 and L_- modes, and the L_+ mode, respectively. The experimental curves in Fig. 10 coincide roughly with the theoretical curves in Fig. 9. This result indicates that the carrier-concentration dependence of the coupled-mode dampings can be qualitatively interrupted by the phonon-content changes.

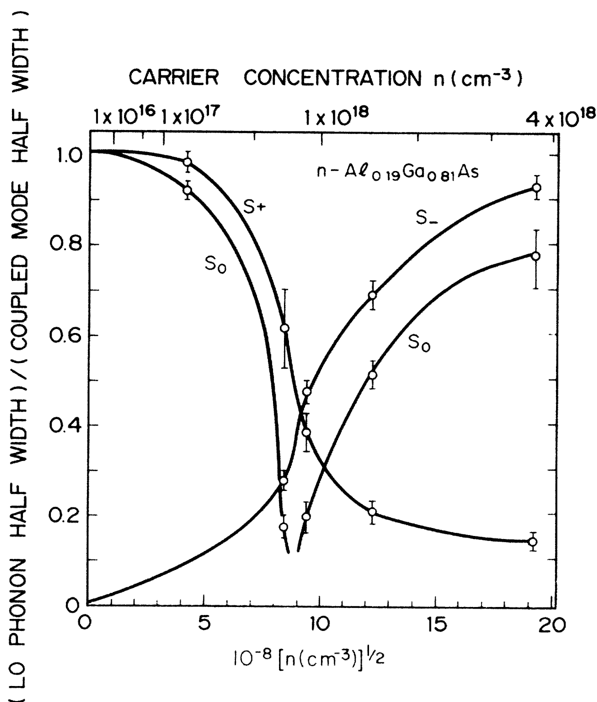

FIG. 10. The reciprocal of the normalized coupled-mode half-widths as a function of the square root of the carrier concentration. For the normalization, the GaAs-like LO-phonon width is used for the L_0 and L_- modes, and the AlAs-like LO-phonon one is used for the L_+ mode.

It is difficult to measure correctly the coupled-mode dampings in the carrier-concentration region with small phonon content, i.e., large plasmon content, because the large plasmon contribution causes the broadening of the coupled modes and leads to difficulty in the observation of the coupled-mode peaks in Raman spectra. Accordingly, the experimental verification of the S_0 minimum in Fig. 9 is very difficult because of the marked broadening. Furthermore, for the L_0 mode, in order to evaluate more accurately the carrier-concentration dependence of the mode strength, the frequencies and oscillator strengths of two LO-phonon branches should be simultaneously considered in Eq. (16).

V. CONCLUSIONS

We have studied in detail Raman scattering from the coupled plasmon—LO-phonon modes in different Si-doped direct-band-gap n-type $Al_xGa_{1-x}As$ grown by molecular-beam epitaxy. The coupled modes, which consist of three branches of the high-frequency, low-frequency, and intermediate-frequency modes, are observed in visibly excited Raman scattering spectra. Their frequencies depend both on the carrier concentration and alloy composition. As the carrier concentration increases, the high-frequency line shifts to the higher-frequency side, becoming separated from the AlAs-like LO phonon, the low-frequency line approaches the GaAs-like TO-phonon position from the lower-frequency side, and the intermediate-frequency line approaches the AlAs-like TO-phonon position, becoming separated from the GaAs-like LO phonon. As the excitation wavelength becomes short, the coupled modes shift to higher frequencies. This wave-vector dependence confirms the assignment to the coupled modes.

The behavior of the coupled modes was analyzed theoretically using the wave-vector-dependent dielectric function of n-type $Al_xGa_{1-x}As$, and the frequencies were calculated as a function of carrier concentration for some excitation wavelengths. The phonon content, which is a measure of the mode strength, was also calculated for the three coupled modes, as a function of carrier concentration. When the carrier concentration increases, the high-frequency-mode strength decreases with decreasing phonon content; in contrast, the low-frequency mode strength increases with increasing phonon content. The intermediate-frequency mode is strengthened at both high and low carrier concentration due to the large phonon content. However, the mode weakens markedly near the carrier concentration at which the peak frequency is equal to the plasma frequency. The observed dampings of the coupled modes vary qualitatively along the calculated carrier-concentration-dependent phonon-content curves. This work can be applied to the other mixed crystals with two-mode behavior.

ACKNOWLEDGMENTS

The present study is part of the national research and development project on optical measurement and control systems, conducted under a program set up by the Agency of Industrial Science and Technology, Ministry of International Trade and Industry, Japan.

APPENDIX

The phonon content of the coupled modes is studied starting from the phonon Green's function, which is defined by

$$D(q,t)=-i\langle 0\,|\,\tau[\varphi_q(t)\varphi_q^\dagger(0)]\,|\,0\rangle \ , \tag{A1}$$

where τ is the time-ordering symbol. In the frequency representation,

$$D(q,\omega)=\sum_m S_m(q)\left[\frac{1}{\omega-\omega_m+i0^+}-\frac{1}{\omega+\omega_m-i0^+}\right] . \tag{A2}$$

On the other hand, expanding D^{-1} near $\omega=\omega_m$, we obtain, for the initial terms,

$$D^{-1}(q,\omega)\sim D^{-1}(q,\omega_m)+[D^{-1}(q,\omega)]'_{\omega=\omega_m}(\omega-\omega_m)+\tfrac{1}{2}[D^{-1}(q,\omega)]''_{\omega=\omega_m}(\omega-\omega_m)^2 . \tag{A3}$$

To express D^{-1} as a function of the frequency ω, we consider the equations of motion for the three atoms. Using the displacement vector $\mathbf{w}$, the equations of motion are written as

$$-\omega^2[M]\mathbf{w}=-\left[\mathbf{K}-\frac{4\pi N}{3}\mathbf{C}\right]\mathbf{w}+\mathbf{e}E \ , \tag{A4}$$

where $[M]$ is the diagonal mass matrix, $\mathbf{e}$ is the charge vector, $\mathbf{K}$ and $(4\pi/3)\mathbf{C}$ are the short-range and dipolar force constants, and N is the number of units or ion pairs per unit volume, which is defined as $4\pi N\alpha=\epsilon_\infty-1$ (α is the electronic polarization per basic unit).

Transforming to the diagonal representation, we have

$$-\omega^2\mathbf{v}=-[\omega^2]\mathbf{v}+\mathbf{e}''E \ , \tag{A5}$$

where

$$[\omega^2]=\begin{bmatrix}\omega_1^2 & 0 & 0\\ 0 & \omega_2^2 & 0\\ 0 & 0 & \omega_3^2\end{bmatrix} , \tag{A6}$$

and $\mathbf{v}$, $\mathbf{e}''$, and ω_j^2 represent the redefined displacement and charge vectors and eigenfrequencies, respectively. In Eq. (A6), two eigenfrequencies ω_1 and ω_2 correspond to the GaAs and the AlAs-like TO-phonon frequencies, respectively, and the third eigenfrequency, ω_3, which corresponds to the $q=0$ acoustic mode, is always zero.

The lattice polarization is given by

$$P_L=N\mathbf{e}''\cdot\mathbf{v}+N\alpha E \ . \tag{A7}$$

From Eqs. (2)–(4), (A7), and $\epsilon_T=0$, the macroscopic field is given by

$$E=-\frac{4\pi N}{4\pi N\alpha+\epsilon_e(q,\omega)}\mathbf{e}''\cdot\mathbf{v} \ . \tag{A8}$$

With Eqs. (A5) and (A8), the frequency squared is given by

$$\omega^2=\omega_{tj}^2+\frac{4\pi N}{\epsilon_e(q,\omega)+\epsilon_\infty-1}(e_j'')^2 \ , \tag{A9}$$

where e_j'' is the element of the charge vector.

Following Eq. (11) of Ref. 1, we obtain

$$\frac{\partial^2}{\partial t^2}D(q,t)=-2\omega_{tj}\delta(t)+\left[-\omega_{tj}^2-\frac{4\pi N}{\epsilon_e(q,\omega)+\epsilon_\infty-1}(e_j'')^2\right]D(q,t) \ . \tag{A10}$$

Upon taking the Fourier time transform on Eq. (A10),

$$D^{-1}(q,\omega)=(2\omega_{tj})^{-1}\left[\omega^2-\left[\omega_{tj}^2+\frac{4\pi N}{\epsilon_e(q,\omega)+\epsilon_\infty-1}(e_j'')^2\right]\right] ,$$

using

$$S_j=4\pi N(e_j'')^2/\omega_{tj}^2=(2\omega_{tj})^{-1}\left[\omega^2-\left[\omega_{tj}^2+\frac{S_j\omega_{tj}^2}{\epsilon_e(q,\omega)+\epsilon_\infty-1}\right]\right] . \tag{A11}$$

From Eqs. (A9) and (A11), $D^{-1}(q,\omega_m)=0$. Therefore, Eq. (A3) becomes

$$D^{-1}(q,\omega)\sim[D^{-1}(q,\omega)]'_{\omega=\omega_m}(\omega-\omega_m)=(2\omega_{tj})^{-1}\left[2\omega_m+\frac{S_j\omega_j^2}{[\epsilon_e(q,\omega)+\epsilon_\infty-1]^2}\left[\frac{\partial\epsilon_e}{\partial\omega}\right]\right]_{\omega=\omega_m} \tag{A12}$$

Comparing Eq. (A2) with Eq. (A12) gives

$$S_m^{-1}(q)=\frac{1}{2\omega_{lj}}\left[2\omega_m+S_j\omega_{tj}^2\frac{1}{[\epsilon_e(q,\omega)+\epsilon_\infty-1]^2}\left[\frac{\partial\epsilon_e}{\partial\omega}\right]\right]_{\omega=\omega_m}. \tag{A13}$$

Equation (16) is obtained from Eqs. (A13) and (8).

[1]B. Varga, Phys. Rev. **137**, A1896 (1965).

[2]K. S. Singwi and M. P. Tosi, Phys. Rev. **147**, 658 (1966).

[3]E. Burstein, A. Pinczuk, and S. Iwasa, Phys. Rev. **157**, 611 (1967).

[4]S. Perkowitz and R. H. Thorland, Solid State Commun. **16**, 1093 (1975).

[5]M. Hashimato and I. Akasaki, Phys. Lett. **25A**, 38 (1967).

[6]A. Pinczuk, G. Abstreiter, R. Trommer, and M. Cardona, Solid State Commun. **21**, 959 (1977).

[7]G. Abstreiter, R. Trommer, M. Cardona, and A. Pinczuk, Solid State Commun. **30**, 703 (1979).

[8]A. Mooradian and G. B. Wright, Phys. Rev. Lett. **16**, 999 (1966).

[9]V. I. Zemski, E. L. Ivchenko, D. N. Mirlin, and I. I. Reshina, Solid State Commun. **16**, 221 (1975).

[10]D. T. Hon and W. L. Faust, Appl. Phys. **1**, 241 (1973).

[11]J. E. Kardontchik and E. Cohen, Phys. Rev. Lett. **42**, 669 (1979).

[12]G. Dionne and J. C. Wooley, Phys. Rev. B **6**, 3898 (1972).

[13]S. W. Mcknight, P. M. Amirtharaj, and S. Perkowitz, Solid State Commun. **25**, 357 (1978).

[14]O. K. Kim and W. G. Spitzer, Phys. Rev. B **20**, 3258 (1979).

[15]T. Yuasa, S. Naritsuka, M. Mannoh, K. Shinozaki, K. Yamanaka, Y. Nomura, M. Mihara, and M. Ishii, Appl. Phys. Lett. **46**, 176 (1985).

[16]Y. Nomura, M. Mannoh, M. Mihara, S. Naritsuka, K. Yamanaka, T. Yuasa, and M. Ishii, J. Electrochem. Soc. **131**, 2630 (1984).

[17]G. Abstreiter, E. Bauser, A. Fisher, and K. Ploog, Appl. Phys. **16**, 345 (1978).

[18]D. L. Rode, J. Appl. Phys. **45**, 3887 (1974).

[19]R. J. Nelson, Appl. Phys. Lett. **31**, 351 (1977).

[20]D. V. Lang, R. A. Logan, M. Jaros, Phys. Rev. B **19**, 1015 (1979).

[21]H. Kunzel, A. Fischer, J. Knecht, and K. Ploog, Appl. Phys. A **32**, 69 (1983).

[22]Miyoko Oku Watanabe, Kouhei Morizuka, Masao Mashita, Yasuo Ashizawa, and Yasuhito Zohta, Jpn. J. Appl. Phys. **23**, L103 (1984).

[23]A. Mooradian and A. L. McWhorter, Phys. Rev. Lett. **19**, 849 (1967).

[24]Yu. I. Ukhanov, Fiz. Tverd. Tela (Leningrad) **5**, 108 (1963) [Sov. Phys.—Solid State **5**, 75 (1963)].

[25]Naresh Chand, Tim Henderson, John Klem, W. Ted Masselink, Russ Fischer, Yia-Chung Chang, and Hadis Morkoç, Phys. Rev. B **30**, 4481 (1984).